Shear Stress Regulation in Cylindrical Arteries through Medial Growth and Nitric Oxide Release

Pak-Wing Fok,
Dept. of Mathematical Sciences,
University of Delaware

December 14, 2022

Abstract

The mechanisms employed by blood vessels in order to adapt to their hemodynamic environment are important for our general understanding of disease and development. Changes in arterial geometry are generally induced by two effects: vasodilation and/or constriction; and growth and remodeling ("G&R"). The first can occur over short periods of a few minutes, while the second usually occurs over timescales of weeks or months. The free radical Nitric oxide (NO) is one of the few biological signaling molecules that is gaseous. When smooth muscle cells internalize NO, they lengthen and ultimately induce a relaxation of the artery. Platelet-Derived Growth Factor (PDGF) is a growth factor released by smooth muscle cells and platelets that regulates cell growth and division.

In this paper we present a single-layered, axisymmetric hyperelastic model for a deforming, growing artery in which the opening angle is regulated by NO and growth is induced by PDGF. Our model describes vasodilation and G&R in a long cylindrical artery regulated by a steady-state Poiseuille flow. The transport of NO released by the endothelium is governed by a diffusion equation with a shear-stress dependent flux boundary condition. Arterial opening angle is assumed to be a Hill function of the wall-averaged NO concentration. We find that both growth and NO help to regulate shear stress with respect to the flow rate, but regulation through growth occurs only at large times. In contrast, regulation through NO is immediate but can only occur as long as the opening angle is able to continually decrease as a function of flow rate. Our model is calibrated using experimental data from ligated, control, and anastomosed carotid arteries of adult and weanling rabbits. Our results generate shear stress/flow rate and lumen radius/flow rate curves that agree with experimental data from control and NO-inhibited rabbit carotid arteries.

1 Introduction

The mechanisms employed by blood vessels in order to adapt to their hemodynamic environment are important for our understanding of cardiac organogenesis (Lindsey et al., 2014)

as well as cardiovascular (Davies, 2009; Ramachandra et al., 2017), ocular (Harris et al., 2013) and even certain cerebral (de la Torre, 2012) diseases. Changes in arterial geometry are broadly induced by two effects: vasodilation/constriction, and growth and remodeling ("G&R"). The first can occur over short periods of a few minutes, while the second usually occurs over timescales of weeks or months. Acute vasodilation/contraction results in a rapid change in vascular *tone* associated with the contractility of smooth muscle cells (SMCs). These changes can usually be reversed (e.g., by applying vasodilators topically), thereby restoring the vessel to its original size. On the other hand, chronic G&R results in permanent or structural changes in vessel morphology which cannot normally be reversed by vasodilators.

Animal experiments such as those of Tronc et al. (1996), and Langille et al. (1989) suggest that medial growth plays a crucial role in experiments where changes in flow do not damage the vessel wall (in contrast, the adventitia plays a more active role when the wall is damaged (Humphrey, 2013)). There are two main ways of altering the flow conditions of arteries *in-vivo*. *Anastomoses* surgically connect a nearby vessel to the vessel under study, thereby increasing the blood flow rate. *Ligations* restrict the flow upstream of the studied vessel, thereby decreasing the flow rate. These flow alteration experiments show that reducing the flow over a long period of time leads to a smaller vessel cross section, with a decreased lumen area. Conversely, an augmented flow gives rise to a larger vessel cross section, with an increased lumen area.

One way to quickly understand these changes in vessel caliber is to assume that the vessel wall adapts in order to maintain a constant shear stress (Struijk et al., 2005). The Poiseuille relation for laminar flow through an infinitely long, cylindrical tube is

$$\tau = \frac{4\mu Q}{\pi b^3}, \tag{1}$$

where τ is shear stress, Q is flow rate, b is lumen radius and μ is the dynamic viscosity of blood. If the vessel adapts to regulate shear stress (i.e. it changes shape to keep shear stress constant) then $b \propto Q^{1/3}$: lumen size increases with flow rate as illustrated by the blue curves in Figure 1. These changes only occur if the flow alterations are sustained over a long time (6-8 months for canine carotid arteries). If the vessel does not adapt, then the artery behaves like a stiff, inert tube with $b =$ constant and $\tau \propto Q$, as illustrated by the red curves in Fig. 1. This "no regulation" limit usually occurs when the vessel does not have sufficient time to grow and remodel, with observations made only a few days into the experiment. When observations are made after a week, the behavior seems to interpolate between the two limiting cases (green markers). Interestingly, there appears to be a breakdown of the $b \propto Q^{1/3}$ scaling for large flow rates even after 6-8 months. According to Kamiya and Togawa (1980), this could be because the artery was unable to grow to the required size within the given timeframe, or it developed pathologies for large flow rates that interfered with adaptation.

While eq. (1) heuristically predicts changes in lumen size when flow conditions are altered, it does not explain morphological changes in terms of underlying biomechanics, which has been the subject of many articles such as Rachev (1997), Alford et al. (2008), Gleason et al. (2004), Mousavi et al. (2019), and Ramachandra et al. (2017). One popular way to describe

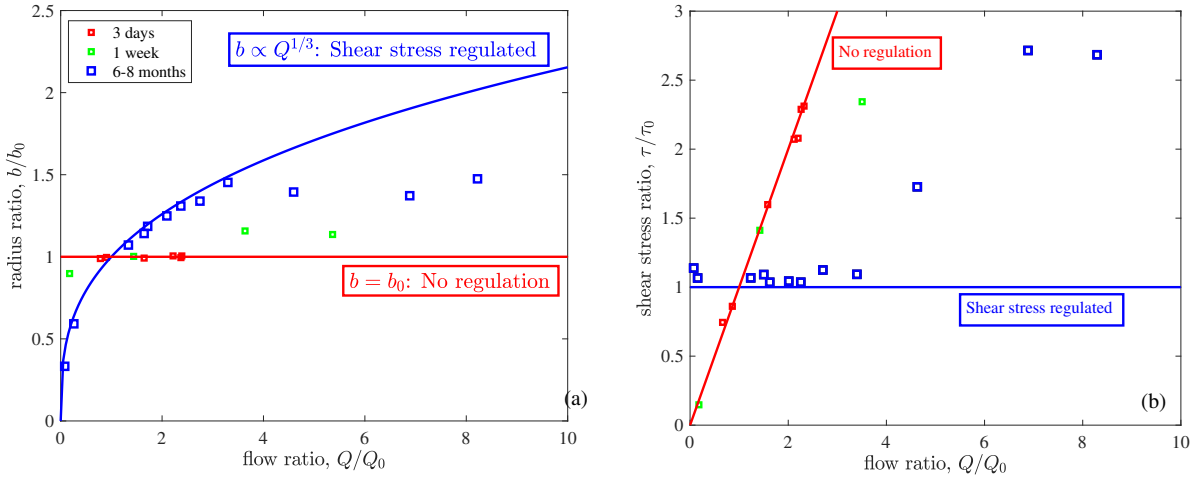

Figure 1: Experimental data for canine carotid arteries showing changes in lumen radius and shear stress as a function of flow rate. Arteries behave in the "no regulation" regime for early times (3 days) and "shear stress regulated" regime for later times (6-8 months). Adapted from Kamiya and Togawa (1980).

how arteries adapt to their hemodynamical environment is through constrained mixture models (Valentin and Humphrey, 2009; Karšaj and Humphrey, 2012). These models assume that the vessel wall is a mix of components such as elastin, collagen and smooth muscle cells, and a total strain energy is formulated as a convex combination of the energies of the individual components. The strength of these models is that they can account for individual turnover of each component as G&R occurs and give detailed information about arterial geometry and internal stresses at any desired time point. However, in most of these models, a homeostatic shear stress is provided as a known input. By construction, the arteries grow and remodel towards their target homeostatic shear stresses.

In this paper we present a single-layered model for a growing artery in which hemodynamic shear stress affects the flux and distribution of Nitric Oxide (NO) in the arterial wall. The single layer represents the media, which is assumed to be an anisotropic hyperelastic material. Anisotropy arises because of the presence of embedded collagen fibers. We incorporate the effect of NO by changing the opening angle ω of the medial layer and account for the effects of Platelet Derived Growth Factor (PDGF) by associating the media with a growth tensor $\mathbf{F}_g$: see Fig. 2. The production of NO is regulated by wall shear stress which is generated by a steady-state Poiseuille flow in the lumen. Growth is described using the "morphoelasticity" framework, decomposing the deformation gradient into a product of a growth tensor and an elastic response (Rodriguez et al., 1994; Goriely, 2017), and the effect of PDGF is modeled indirectly by assuming an algebraic relationship between the growth tensor and flow rate. In contrast to mixture models, the homeostatic shear stress is a product of our model, rather than an input.

The endothelium acts as a mechano-sensor of shear stress: by releasing signaling factors

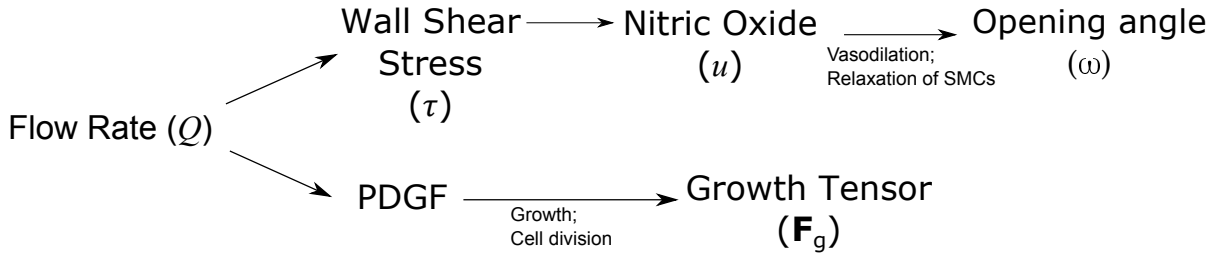

Figure 2: Effect of NO and PDGF on vasomotion and growth and remodeling (G&R). A greater shear stress induces more rapid release of NO which relaxes the artery. A larger flow rate induces more PDGF to be released from SMCs which promotes cell proliferation and growth.

such as VEGF, eNOS and PDGF into the vessel wall, endothelial cells influence the behavior of smooth muscle cells, effectively acting as mediators of vessel tone and geometry. By accounting for how these signaling factors are transported and distributed, and by making some assumptions about how SMCs proliferate and contract in response to these signals, we find that the regulation of shear stress is a mathematical consequence of the model, with the homeostatic shear stress depending on biophysical factors such as rate of medial growth, axial stretch, and lumen pressure.

This paper is organized as follows: in section 2 we derive and present the governing equations for an artery undergoing axisymmetric deformations. The equations are standard and can be skipped by readers familiar with hyperelasticity theory, but the inclusion of NO-mediated relaxation in section 2.2.4 is new, to the author's knowledge. In addition, in section 2.2.5 we show that our growth model admits an exact solution that produces the characteristic $Q^{1/3}$ scaling seen in experiments. In section 3 we determine the parameters of our model and explore how shear stresses are regulated for the cases of pure growth, pure vasodilation, and joint growth and vasodilation by making connections to published experimental data. We end with a conclusion in section 4.

2 Governing Equations

2.1 Assumptions of the Model

We focus on modeling the media since it is the layer that is mainly responsible for actively regulating the artery (Humphrey, 2013), and its dimensions are directly measured in experiments. The mechanical properties of the adventitia can be included but we do not model the outer layer in this paper. Including the adventitia significantly complicates the model since both the media and adventitia in their separated, unstressed reference configurations would have their own opening angles. We ignore the intima because in flow-alteration experiments, there is insignificant intimal growth. Therefore we are primarily concerned with the lumen-media interface and the outer boundary of the media. These interfaces are described by two radii b and c.

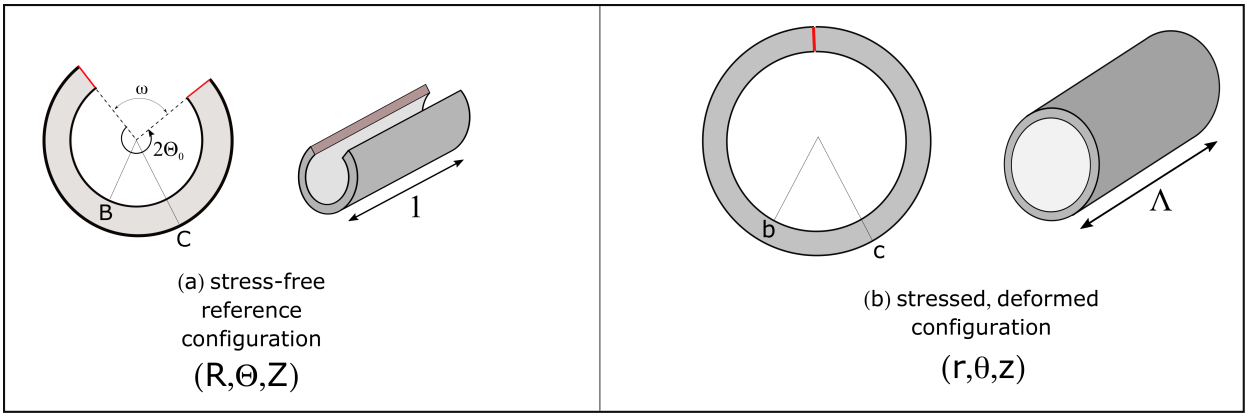

Figure 3: A stress-free arterial segment (a) is mapped to a residually-stressed arterial cross-section (b). The lumen in (b) may be pressurized. The angles ω and Θ_0 are related by $\omega = 2\pi - 2\Theta_0$. A uniform stretch Λ is applied in the axial direction.

A deformation takes the segment parameterized by (R, Θ, Z) to a full annulus parameterized by (r, θ, z): see Fig. 3. We assume an axisymmetric deformation

$$r = r(R), \qquad B \le R \le C, \tag{2}$$

$$\theta = \frac{\pi\Theta}{\Theta_0(\langle u \rangle)}, \qquad 0 \le \Theta \le 2\Theta_0, \tag{3}$$

$$z = \Lambda Z, \qquad -\infty \le Z \le \infty, \tag{4}$$

with corresponding opening angle $\omega \equiv 2\pi - 2\Theta_0(\langle u \rangle)$. To be consistent with axisymmetric deformations, the pressure along the artery must be constant with respect to z. This is obviously a simplification but within the framework of 2D models, it is quite standard (Humphrey, 2013). Classical studies on human femoral arteries have reported a mean pressure drop of about 5 mmHg per 60 cm of axial length (Raines et al., 1974) so the assumption of constant lumen pressure is not unreasonable. All quantities will ultimately depend on time t when growth is introduced, but for simplicity we omit the dependence on t in the model derivation.

We now discuss our main modeling assumptions.

1. *Opening angle depends on wall-averaged concentration of NO.* Experiments on rat aortas suggest that the opening angle can depend on vasoactive agents (e.g. see Fig. 2 of Matsumoto et al. (1996)). As a simplification, we assume that the opening angle of the vessel wall depends on the *wall-averaged* concentration of these agents:

$$\langle u \rangle = \frac{2}{c^2 - b^2} \int_b^c u(r) r dr.$$

While it would be ideal to have opening angle depend on pointwise concentrations, defining a single opening angle for an arterial section with spatially dependent NO

becomes very difficult. The wall-average assumption allows us to write down a relatively simple model that can be more easily analyzed, and still describe a wide range of observed behaviors.

2. *Nitric Oxide changes mainly the opening angle ω and changes in radii B and C are assumed to be small.* In other words, NO causes mainly circumferential lengthening, and very little bending in the reference configuration. This would be a reasonable assumption if the wall is thin and SMCs contract by the same amount on the inner and outer surfaces of the wall. Another way of stating this is that the strain in the media is uniform across its thickness and this uniformity does not change in the presence of NO.

3. *Configuration (a) in Fig. 3 exists in a stress-free state.* By allowing Θ_0 to depend on $\langle u \rangle$, we assume the length of SMCs depends on $\langle u \rangle$. In the presence of a vasodilator, SMCs relax and reduce the opening angle ω in Fig. 3(a), thereby decreasing the tension in the stressed state (b). Equivalently, Θ_0 increases with $\langle u \rangle$. For example, when $\Theta_0 \to \pi$, there is no residual stress in (b). The contractile apparatus within a SMC allows it to pull on its neighbors and this can occur in both states in Fig. 3 (a) and (b). The pulling would increase ω in the cut segment (a) but increase circumferential stress in (b). Under the action of NO, the area of the cross section in (a) reduces as ω increases, but the segment lengthens in the Z direction to conserve mass.

4. *PDGF and NO do not interact.* NO has also been shown to downregulate PDGF (Yu et al., 2012), but in this paper we assume that PDGF only induces growth and ignore any interactions between NO and PDGF. There is evidence that PDGF can also change muscle tone, but whether a contraction or relaxation occurs depends on which isoform is present (Berk et al., 1986).

5. *Growth in the radial and circumferential directions is isotropic.* We will assume that growth in the media depends algebraically on the flow rate Q, that there is no growth in the axial direction, and that growth is isotropic in the radial and circumferential directions, so $g_r = g(Q,t)$, $g_\theta = g(Q,t)$ and $g_z = 1$. However, we derive the governing equations in section 2.2.1 for general g_r, g_θ, g_z.

Most authors do not model SMC contraction by allowing Θ_0 to depend on $\langle u \rangle$. In the literature, it is common to account for SMC contraction by making assumptions directly about the *circumferential stress*. Classical experiments such as Cox (1975) have indicated that different vasoactive agents such as norepinephrine or potassium chloride produce different pressure-diameter relationships and most modeling efforts postulate some algebraic relationship between stress and strain, including SMC contraction as a shape parameter. For example, Rachev and Hayashi (1999) assume that the circumferential stress can be written as the sum of passive and active stresses, and include an additional parameter in the active stress term to control SMC contraction. In contrast, we describe SMC contraction by manipulating the reference, stress-free state. Our model connects more closely with the experiments of Matsumoto et al. (1996) who show a change in opening angle when vasodilators/vasocontractors are applied.

2.2 Model Derivation

2.2.1 Kinematics

In flow-alteration experiments, there can be significant growth of the media and we wish to accommodate an expansion of medial cross-sectional area. Morphoelasticity assumes that the deformation gradient is a product of an elastic tensor and a growth tensor (Rodriguez et al., 1994). In addition, we assume the artery is incompressible, so we have

$$\mathbf{F} = \mathbf{F}_e\mathbf{F}_g, \qquad \det \mathbf{F}_e = 1, \qquad \mathbf{F}_g = \mathrm{diag}(g_r, g_\theta, g_z), \tag{5}$$

where $\mathbf{F}$ is the deformation gradient, $\mathbf{F}_e$ is the elastic tensor, $\mathbf{F}_g$ is the growth tensor, and g_r, g_θ and g_z are the growth ratios in the radial, circumferential, and axial directions. A growth ratio of 1 signifies no growth, whereas a ratio > 1 (< 1) signifies an increase (decrease) in mass. Assuming axisymmetric deformations (2)-(4), the deformation gradient in cylindrical coordinates simplifies to

$$\mathbf{F} = \begin{pmatrix} r'(R) & 0 & 0 \\ 0 & \frac{\pi r}{\Theta_0 R} & 0 \\ 0 & 0 & \Lambda \end{pmatrix}. \tag{6}$$

In rabbits and dogs, carotid arteries appear to be axially stretched with an *in-vivo* length $\sim 1.6\times$ their excised length (Doyle and Dobrin, 1971; Jackson et al., 2002). Therefore we take $\Lambda = 1.6$. The morphoelasticity decomposition eq. (5) implies

$$\begin{pmatrix} r' & 0 & 0 \\ 0 & \frac{\pi r}{\Theta_0 R} & 0 \\ 0 & 0 & \Lambda \end{pmatrix} = \begin{pmatrix} \alpha_r & 0 & 0 \\ 0 & \alpha_\theta & 0 \\ 0 & 0 & \alpha_z \end{pmatrix} \begin{pmatrix} g_r & 0 & 0 \\ 0 & g_\theta & 0 \\ 0 & 0 & g_z \end{pmatrix}, \tag{7}$$

where α_r, α_θ and α_z are elastic stretches in the radial, circumferential, and axial directions. Equating components,

$$r' = \alpha_r g_r, \tag{8}$$

$$\frac{\pi r}{\Theta_0 R} = \alpha_\theta g_\theta, \tag{9}$$

$$\Lambda = \alpha_z g_z, \tag{10}$$

which implies

$$\alpha_\theta \equiv \alpha = \frac{\pi r}{\Theta_0 R g_\theta}, \tag{11}$$

$$\alpha_z = \frac{\Lambda}{g_z}. \tag{12}$$

Because $\det \mathbf{F}_e = 1$, we have $\alpha_r\alpha_\theta\alpha_z = 1$, or

$$\alpha_r = \frac{1}{\alpha_\theta\alpha_z} = \frac{g_z}{\alpha\Lambda}, \tag{13}$$

which allows us to write the elastic tensor as $\mathbf{F}_e = \text{diag}\left(\frac{g_z}{\Lambda\alpha}, \alpha, \frac{\Lambda}{g_z}\right)$. The ODE for the deformation is

$$\frac{\mathrm{d}r}{\mathrm{d}R} = \frac{g_z}{\alpha\Lambda} g_r = \frac{R}{r} \cdot \frac{\Theta_0}{\pi\Lambda} \cdot g_r g_\theta g_z \tag{14}$$

$$\Rightarrow \int_b^r r' dr' = \frac{\Theta_0}{\pi\Lambda} \int_B^R g_r g_\theta g_z R' dR' \tag{15}$$

$$\Rightarrow r(R) = \left(b^2 + \frac{\Theta_0 g_r g_\theta g_z}{\pi\Lambda} (R^2 - B^2) \right)^{1/2}, \qquad B < R < C. \tag{16}$$

With $r(R)$ prescribed, eq. (11) defines a circumferential stretch in terms of the reference radial coordinate: $\alpha(R) = \pi r(R)/(\Theta_0 R g_\theta)$. Alternatively, if (16) is inverted to yield $R(r)$, the circumferetial stretch can also be written in terms of the *deformed* radial coordinate: $\alpha(r) = \pi r/(\Theta_0 R(r) g_\theta)$. Since $r(C) = c$, the deformed radii b and c must satisfy

$$c^2 - b^2 - \frac{\Theta_0 g_r g_\theta g_z}{\pi\Lambda} (C^2 - B^2) = 0. \tag{17}$$

2.2.2 Mechanical properties of the media

We describe the mechanical properties of the media using the HGO (Holzapfel-Gasser-Ogden) strain energy (Holzapfel et al., 2005):

$$W = \mu_0 (I_1 - 3) + \frac{\eta}{\beta} \left[e^{\beta (I_4 - 1)_+^2} - 1 \right], \tag{18}$$

$$I_1 = \alpha_r^2 + \alpha_\theta^2 + \alpha_z^2 = \frac{g_z^2}{\Lambda^2} \alpha^{-2} + \alpha^2 + \frac{\Lambda^2}{g_z^2}, \tag{19}$$

$$I_4 = \alpha_\theta^2 \cos^2\varphi + \alpha_z^2 \sin^2\varphi = \alpha^2 \cos^2\varphi + \frac{\Lambda^2}{g_z^2} \sin^2\varphi. \tag{20}$$

The mechanical parameters μ_0, η and β can be inferred from stress-strain experiments: see Table 1 for measured values in a rabbit carotid artery. The angle φ describes the orientation of helical collagen fibers embedded within the media. There are actually two families of these fibers, but because they are symmetrically inclined at $-\pi/2 + \varphi$ and $\pi/2 - \varphi$ with respect to the axial direction, both families can be mathematically represented by a single exponential function in eq. (18). Note that $x_+ \equiv \max(x, 0)$ and the quantity I_4 is interpreted as the normalized length of deformed collagen fibers: $I_4 > 1$ means the fibers are stretched whereas $I_4 < 1$ means they are compressed. The reason for using $(I_4 - 1)_+^2 \equiv [(I_4 - 1)_+]^2$ in (18) rather than $(I_4 - 1)^2$ is that these fibers only contribute to the strain energy when they are stretched. Because the strain energy in (18) is only a function of circumferential stretch α, we define

$$w(\alpha) = \mu_0 (I_1 - 3) + \frac{\eta}{\beta} \left[e^{\rho (I_4 - 1)_+^2} - 1 \right] \tag{21}$$

$$\Rightarrow \frac{1}{\alpha} \frac{\mathrm{d}w}{\mathrm{d}\alpha} \equiv H(\alpha), \tag{22}$$

Symbol	Meaning	Value
μ_0	mechanical parameter for ground substance	1.5 kPa
η	mechanical parameter for collagen fibers	2.36 kPa
β	mechanical parameter for collagen fibers	0.84
φ	media fiber angle	29.0°

Table 1: Model parameters for the media layer in a rabbit carotid artery. The strain energy (18) is composed of terms for ground substance and collagen fibers. Values are taken from Holzapfel et al. (2001).

and $H(\alpha)$ is defined as

$$\begin{aligned} H(\alpha) &= \frac{\mu_0 I_1'(\alpha)}{\alpha} + 2\eta \cdot \frac{(I_4-1)_+ I_4'(\alpha)}{\alpha} e^{\beta(I_4-1)_+^2}, \\ &= 2\mu_0 \left(1 - \frac{g_z^2 \alpha^{-4}}{\Lambda^2}\right) + 4\eta \left[(I_4-1)_+ \cos^2\varphi\right] e^{\beta(I_4-1)_+^2}. \end{aligned} \tag{23}$$

2.2.3 Stress and Equilibrium

In axially uniform, axisymmetric morphoelasticity, the strain energies are functions of the geometric stretches α_r and α_θ but because of the relation (13), the radial and circumferential stretches are inversely proportional to each other. Therefore:

$$dw = \frac{\partial W}{\partial \alpha_r} d\alpha_r + \frac{\partial W}{\partial \alpha_\theta} d\alpha_\theta, \tag{24}$$

$$\Rightarrow \frac{dw}{d\alpha_\theta} = \frac{\partial W}{\partial \alpha_r}\left(-\frac{g_z}{\Lambda \alpha_\theta^2}\right) + \frac{\partial W}{\partial \alpha_\theta}, \tag{25}$$

$$\Rightarrow \alpha_\theta \frac{\mathrm{d}w}{\mathrm{d}\alpha_\theta} = \alpha_\theta \frac{\partial W}{\partial \alpha_\theta} - \alpha_r \frac{\partial W}{\partial \alpha_r}. \tag{26}$$

The stress-strain relation for an incompressible hyperelastic material is

$$T_{rr} = \alpha_r \frac{\partial W}{\partial \alpha_r} - p, \qquad T_{\theta\theta} = \alpha_\theta \frac{\partial W}{\partial \alpha_\theta} - p, \qquad T_{zz} = \alpha_z \frac{\partial W}{\partial \alpha_z} - p, \tag{27}$$

where p is the hydrostatic pressure and acts as a Lagrange multiplier. Mechanical equilibrium implies $\nabla \cdot \mathbf{T} = 0$ where $\mathbf{T}$ is the Cauchy stress tensor. The only non-vanishing component of the momentum equation is

$$\frac{\partial T_{rr}}{\partial r} + \frac{T_{rr} - T_{\theta\theta}}{r} = 0. \tag{28}$$

This equation is supplemented by boundary conditions

$$T_{rr}(r=b) = -P, \tag{29}$$

$$T_{rr}(r=c) = 0, \tag{30}$$

where P is the lumen pressure. Eq. (30) is a simplification and assumes the outer boundary of the media is traction-free. In reality, the media is surrounded by the adventitial layer and T_{rr} would need to be continuous across the media-adventitia interface. Using (26), (27), (28), the radial stress satisfies

$$\begin{aligned} \frac{\partial T_{rr}}{\partial r} &= \frac{1}{r}\left(\alpha_\theta \frac{\partial W}{\partial \alpha_\theta} - \alpha_r \frac{\partial W}{\partial \alpha_r}\right) = \frac{\alpha}{r}\frac{\mathrm{d}w}{\mathrm{d}\alpha}, \\ \Rightarrow T_{rr}(r) &= -P + \int_b^r \frac{\alpha(r')}{r'}\frac{\mathrm{d}w}{\mathrm{d}\alpha} dr', \end{aligned}$$

and the pressure condition (29) has been satisfied. Zero traction at $r = c$, represented by eq. (30) gives

$$-P + \int_b^c \frac{\alpha(r')}{r'}\frac{\mathrm{d}w}{\mathrm{d}\alpha}\mathrm{d}r' = 0. \tag{31}$$

Using eqs. (11) and (14), the transformation from the reference frame to the deformed frame $r(R)$ satisfies $\alpha^2 dr/r = (g_r g_z \pi)/(g_\theta \Lambda \Theta_0) dR/R$. Using eq. (22), the traction-free boundary condition (31) becomes

$$-\frac{P\Theta_0\Lambda}{\pi} + \frac{g_r g_z}{g_\theta}\int_B^C H[\alpha(R')]\frac{\mathrm{d}R'}{R'} = 0. \tag{32}$$

Given the radial stress, the hoop stress distribution immediately follows:

$$\begin{aligned} T_{\theta\theta} &= r\frac{\partial T_{rr}}{\partial r} + T_{rr}, & (33)\\ &= \alpha\frac{\mathrm{d}w}{\mathrm{d}\alpha} + T_{rr}, & (34)\\ &= \alpha^2 H(\alpha) + T_{rr}, & (35)\\ &= -P + \alpha^2 H(\alpha) + \int_b^r \alpha^2(r') H[\alpha(r')]\frac{dr'}{r'}. & (36) \end{aligned}$$

2.2.4 Nitric Oxide Transport

Nitric oxide (NO) or endothelium-derived relaxing factor is a free radical and one of the few biological signaling molecules that is gaseous. It is synthesized in endothelial cells and acts as an intercellular messenger. NO is highly reactive and is quickly taken up by smooth muscle cells. When smooth muscle cells internalize NO, they lengthen and ultimately induce a relaxation of the artery. Biomechanically, we model the relaxation by reducing the residual hoop stress in the arterial wall in Fig 3(b) and allowing the opening angle ω in Fig. 3(a) to depend on the wall-averaged NO concentration.

Let u be the extracellular concentration of NO. NO diffuses, reacts with oxygen and is taken up by cells. The average rate of NO depletion can, in principle, be different depending on the cellular environment. For example, if there is a greater density of cells, the uptake would be greater. In our model, we assume that NO diffuses and is taken up by cells and/or

reacts to form by-products at a constant rate. If the degradation rate is much faster than the uptake rate by cells, then at steady state, we have

$$\frac{D_{NO}}{r}\frac{\partial}{\partial r}\left(r\frac{\partial u}{\partial r}\right) - ku = 0, \qquad r > b, \tag{37}$$

where $D_{NO} \approx 3400\ \mu\text{m}^2/s$ is the diffusivity of NO and $k \approx 0.17/s$ assuming that the half-life of NO is 4 seconds (Lancaster, 1994). Having cells take up NO at a rate comparable to or greater than the reaction rate with oxygen amounts to using different values for k – see the Appendix. The production rate of NO depends on the wall shear stress experienced by endothelial cells, so we take the boundary conditions of eq. (37) to be

$$-D_{NO}\left.\frac{\partial u}{\partial r}\right|_{r=b} = q_{\text{ref}} f(\tau), \tag{38}$$

$$u(r \to \infty) = 0. \tag{39}$$

For the boundary condition at $r = b$, a rough estimate of the typical NO production rate (per unit surface area of endothelium) is $q_{\text{ref}} = 5 \times 10^{-20}$ mol/μm^2/s. This value was found by Vaughn et al. (1998) in a theoretical model of endothelial NO release. While eqs. (37)-(39) are defined on a semi-infinite domain (b, ∞), we are only interested in $u(r)$ on $b \le r \le c$.

Motivated by the data and terminology from Humphrey (2008), f is a *mechanical dose response* curve and τ is the wall shear stress. Figure 8 from this paper motivates a saturating function for f:

$$f(\tau) = p_1 + p_2(1 - \exp(-p_3\tau^2)). \tag{40}$$

Generally, vessels maintain a basal level of NO so we expect $p_1 \ge 0$. For f to be monotonically increasing and saturate for large τ, we also require $p_2, p_3 > 0$. Data on bovine aortic endothelial cells suggests $p_1 \approx 0.35$, $p_2 \approx 0.65$, $p_3 \approx 8.6$ Pa^{-2} (Humphrey, 2008) but in section 3.1.2 we will infer p_1, p_2 and p_3 for rabbit carotid endothelium. At steady state, the solution to (37)-(39) is

$$u(r) = \frac{q_{\text{ref}} f(\tau)}{\lambda D_{NO} K_1(\lambda b)} K_0(\lambda r), \qquad \lambda = \sqrt{k/D_{NO}},$$

where $K_0(\cdot)$ is a modified Bessel function of the second kind. In the simple case of steady state Poiseuille flow through a long tube of radius b, the shear stress induced by a Newtonian fluid is given exactly by

$$\tau = \frac{4\mu}{\pi}\frac{Q}{b^3}, \tag{41}$$

where μ is the dynamic viscosity of the fluid and Q is the flow rate with units of volume per unit time. We assume that the opening angle of the media depends on the wall-averaged NO concentration, so $\omega = \omega(\langle u \rangle)$ with

$$\omega(\langle u \rangle) = \omega_{\max} - (\omega_{\max} - \omega_{\min})\frac{\langle u \rangle^M}{U^M + \langle u \rangle^M}, \tag{42}$$

where U is the concentration required to achieve 50% "activation," resulting in an opening angle of $(\omega_{\max} + \omega_{\min})/2$. If we assume the opening angle depends on a Hill function of *intracellular* NO, we still obtain eq. (42): see the Appendix for details. For the rest of this paper, we take $M = 2$. This is an arbitrary choice; the main property that $\omega(\langle u \rangle)$ should satisfy is for $\omega = \omega_{\max}$ at $\langle u \rangle = 0$ and $\omega \to \omega_{\min}$ as $\langle u \rangle / U \to \infty$. The wall-averaged NO concentration is

$$\langle u \rangle = \frac{2K_1^{-1}(\lambda b)}{(c^2 - b^2)} \frac{q_{\text{ref}} f(\tau)}{\lambda D_{NO}} \int_b^c r K_0(\lambda r) dr. \tag{43}$$

For ease of infering parameters in later sections, eq. (43) can also be rewritten in terms of a normalized concentration:

$$n = \frac{\langle u \rangle}{U} = \frac{2q_{\text{ref}} f(\tau)}{\lambda D_{NO} U} \cdot \frac{K_1^{-1}(\lambda b)}{(c^2 - b^2)} \int_b^c r K_0(\lambda r) dr. \tag{44}$$

Since we assumed that growth in the media depends algebraically on the flow rate Q, that there is no growth in the axial direction, and that growth is isotropic in the radial and circumferential directions, $g_r = g(Q,t)$, $g_\theta = g(Q,t)$ and $g_z = 1$. When these growth functions are known, the full model is described by the five equations

$$c^2 - b^2 - \left(1 - \frac{\omega}{2\pi}\right) \frac{g^2(Q,t)(C^2 - B^2)}{\Lambda} = 0, \tag{45}$$

$$-P\Lambda \left(1 - \frac{\omega}{2\pi}\right) + \int_B^C H[\alpha(R')] \frac{\mathrm{d}R'}{R'} = 0, \tag{46}$$

$$n - \frac{2K_1^{-1}(\lambda b)}{(c^2 - b^2)} \frac{q_{\text{ref}}(p_1 + p_2(1 - e^{-p_3 \tau^2}))}{\lambda D_{NO} U} \int_b^c r K_0(\lambda r) dr = 0, \tag{47}$$

$$\omega - \omega_{\max} + (\omega_{\max} - \omega_{\min}) \frac{n^2}{1 + n^2} = 0, \tag{48}$$

$$\tau - \frac{4\mu Q}{\pi b^3} = 0, \tag{49}$$

which relate to the deformation of the artery (eq. (17)), a traction-free outer boundary for a vessel under mechanical equilibrium (eq. (32)), the normalized mean NO concentration in the vessel wall (eq. (44)), the opening angle in terms of normalized NO (eq. (42) with the choice $M = 2$), and the definition of shear stress (eq. (41)). Furthermore, in eq. (46), $\alpha(R) = \frac{\pi r(R;b)}{\Theta_0 R g_\theta}$ from eq. (11) with $r(R)$ defined by eq. (16). The five symbols b, c, n, ω and τ can be treated as the unknown variables for a given flow rate Q and time t. In other words, given a particular growth function $g(Q,t)$, and given the mechanical properties of the artery and the transport properties of NO, solving the forward problem (45)-(49) yields the inner and outer radii b, c; the dimensionless NO level n; the opening angle ω; and the shear stress τ. In the next section, we derive a possible algebraic form for $g(Q,t)$.

2.2.5 Flow-rate dependent growth law

Consider a case with pure growth of the form $g_r = g_\theta = g$, $g_z = 1$ and no vasodilation so that $\omega =$ constant in eqs. (45)-(49) The only unknowns are b and c which satisfy

$$c^2 - b^2 - \left(1 - \frac{\omega}{2\pi}\right)\frac{g^2(C^2 - B^2)}{\Lambda} = 0, \tag{50}$$

$$-P\Lambda\left(1 - \frac{\omega}{2\pi}\right) + \int_B^C H[\alpha(R')]\frac{\mathrm{d}R'}{R'} = 0, \tag{51}$$

where H is defined by eq. (23) and

$$r(R) = \left(b^2 + \frac{\Theta_0 g^2}{\pi\Lambda}(R^2 - B^2)\right)^{1/2}, \tag{52}$$

$$\alpha(R) = \frac{\pi r(R;b)}{\Theta_0 R g}, \tag{53}$$

from eqs. (16) and (11) respectively.

Lemma 1. *Let b_0, c_0 satisfy the equations*

$$c_0^2 - b_0^2 - \left(1 - \frac{\omega}{2\pi}\right)\frac{(C^2 - B^2)}{\Lambda} = 0, \tag{54}$$

$$-P\Lambda\left(1 - \frac{\omega}{2\pi}\right) + \int_B^C H[\alpha_0(R')]\frac{dR'}{R'} = 0, \tag{55}$$

with corresponding radial deformation and circumferential stretch

$$r_0(R) = \left(b_0^2 + \frac{\Theta_0}{\pi\Lambda}(R^2 - B^2)\right)^{1/2}, \tag{56}$$

$$\alpha_0(R) = \frac{\pi r_0(R)}{\Theta_0 R}. \tag{57}$$

In other words, b_0, c_0, $r_0(R)$ and $\alpha_0(R)$ are a solution to the pressurized annulus problem, eqs. (50) and (51). Then for any constant $g > 0$, the grown radii, deformation and circumferential stretch

$$b = b_0 g, \tag{58}$$

$$c = c_0 g, \tag{59}$$

$$r(R) = r_0(R) g, \tag{60}$$

$$\alpha(R) = \alpha_0(R), \tag{61}$$

also satisfy equations (50) and (51).

Proof. By direct substitution,

$$c^2 - b^2 - \left(1 - \frac{\omega}{2\pi}\right)\frac{g^2(C^2 - B^2)}{\Lambda} \tag{62}$$

$$= g^2 \underbrace{\left[c_0^2 - b_0^2 - \left(1 - \frac{\omega}{2\pi}\right)\frac{(C^2 - B^2)}{\Lambda}\right]}_{=0} \tag{63}$$

$$= 0, \tag{64}$$

so eq. (50) is satisfied. Note that since α is dimensionless in eq. (61) (unlike b, c and r), it remains invariant when all radii are scaled by g, and so eq. (51) is automatically satisfied:

$$-P\Lambda\left(1 - \frac{\omega}{2\pi}\right) + \int_B^C H[\alpha_0(R')]\frac{\mathrm{d}R'}{R'} \tag{65}$$

$$= -P\Lambda\left(1 - \frac{\omega}{2\pi}\right) + \int_B^C H[\alpha(R'; b)]\frac{\mathrm{d}R'}{R'} \tag{66}$$

$$= 0. \quad \square \tag{67}$$

Now suppose we allow $g = g(Q)$ so the growth depends on flow rate Q. The following corollary describes a simple class of growth functions that keep the shear stress invariant with respect to the flow rate.

Corollary 1. *If $b = b_0$ and $c = c_0$ satisfy eqs. (50) and (51) when $g = 1$, then $b = b_0 g$ and $c = c_0 g$ with $g(Q) = (Q/Q_0)^{1/3}$, where Q is the flow rate, also satisfy eqs. (50) and (51) for any constant Q_0 and the corresponding shear stress is*

$$\tau = \frac{4\mu Q}{\pi b^3} = \frac{4\mu Q}{\pi b_0^3 g^3} = \frac{4\mu Q_0}{\pi b_0^3}, \tag{68}$$

which is independent of Q. Hence the growth law $g = (Q/Q_0)^{1/3}$ induces a change in arterial radius that maintains a constant shear stress equal to $4\mu Q_0/(\pi b_0^3)$.

The constant Q_0 represents how quickly g increases as Q increases (smaller Q_0 means g increases more rapidly). Therefore, the homeostatic shear stress in (68) depends on the deformed radius b_0, when growth is absent, as well as how quickly the media grows with respect to Q, which is captured by the constant Q_0. Note that b_0, in turn, depends on lumen pressure P, axial stretch Λ, opening angle ω and the mechanical properties of the media.

As shown in Fig. 1, shear stress constancy only occurs when the flow experiments are performed over a sufficiently long time. At early times, there is no regulation and arterial radius is constant with respect to Q. This suggests introducing a time-dependence in the growth law so that $g \sim (Q/Q_0)^{1/3}$ as $t \to \infty$ but $g = 1$ at $t = 0$. We can interpolate through both of these behaviors using the simple relation

$$g(Q, t) = \left(\frac{Q}{Q_0}\right)^{1/3} + \left[1 - \left(\frac{Q}{Q_0}\right)^{1/3}\right] e^{-t/T}, \tag{69}$$

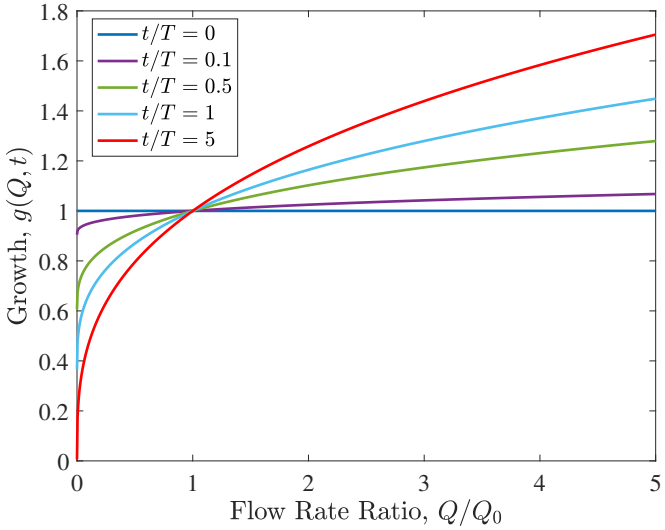

Figure 4: Growth as a function of flow rate and time: see eq. (69). For early times $t/T \approx 0$ there is no growth whereas for later times $t/T \gg 1$, $g \propto Q^{1/3}$.

where T is a growth and remodeling time scale which could be on the order of 6-8 months for canine carotids (Kamiya and Togawa, 1980). Some representative forms of $g(Q,t)$ are shown in Fig. 4. We use this algebraic form for $g(Q,t)$ to supplement eqs. (45)-(49) in the following sections.

3 Results and Connection with Experiments

We will consider three groups of flow-alteration experiments performed on rabbit carotid arteries. In every group, the flow rate is altered by ligations or anastomoses; however the vasoactive and growth properties of the arteries are different from group to group.

In the first case, we consider an artery deforming under pure vasodilation. Experimentally, adult rabbit arteries do not grow significantly when flow conditions are altered. However, their arteries still undergo deformation and vasodilation as flow conditions are altered. In the second case, we consider an artery deforming under pure growth. In experiments, the media cross sectional areas of weanling rabbit arteries change substantially, compared to adult rabbits, when local flow conditions are altered. Furthermore, NO production can be suppressed by adding L-NAME (L-arginine-methyl ester) to their drinking water, so vasodilation can be assumed to play little or no role. In the third and final case, we consider an artery deforming under both growth and vasodilation. This is a suitable model to describe the growth and deformation of the arteries in weanling rabbits. Without any additional treatments, their arteries are able to undergo normal vasodilation, and because the rabbits are young, the media undergoes significant growth.

Quantity	Control	Ligated	Anastomosed
Perfusion pressure, P (mmHg)	100	100	100
Lumen Radius (mm)	$b_{C,data} = 0.88$	$b_{L,data} = 0.7$	$b_{A,data} = 0.93$
Media CSA (mm^2)	$M_{C,data} = 0.35$	$M_{L,data} = 0.32$	$M_{A,data} = 0.35$
Flow Rate (mm^3/s)	$Q_{C,data} = 868$	$Q_{L,data} = 333$	$Q_{A,data} = 1367$

Table 2: Hemodynamic data for common carotid arteries, taken from two studies of flow alteration experiments on adult New Zealand White Rabbits. $M_{C,data}$, $M_{L,data}$, $b_{C,data}$ and $b_{L,data}$ are taken from Fig. 3 of Langille et al. (1989) while $b_{A,data}$,$M_{A,data}$ are taken from Figs. 2 and 3 of Lee and Langille (1991). The flow rates are taken from the "Response to increased blood flow" section on page 980 and Fig. 4 of Lee and Langille (1991).

3.1 Pure Vasodilation in Adult Rabbit Arteries

3.1.1 Inferring the Reference State Configuration

Lee and Langille (1991) and Langille et al. (1989) performed ligation and anastomosis experiments on adult rabbit carotids and measured the associated geometric changes in the arterial cross section. The results are summarized in Table 2. The arteries in adult rabbits typically do not experience much growth when the flow is changed, evidenced by the media cross sectional area (CSA) remaining approximately constant compared to controls. With $g = 1$, equations (45)-(46) decouple from (47)-(49) and may be solved first to find suitable reference radii B, C and opening angle ω. After the parameters of the reference configuration are established, we calibrate against hemodynamic data to find the parameters of the NO-release model.

Phrased as a forward problem, eqs. (45) and (46) constitute 2 equations in the 2 unknowns b and c, providing the opening angle ω or Θ_0 are known, along with the lumen pressure P, axial stretch Λ, and reference radii B and C. However, the arteries of control, ligation, and anastomosis experiments are vasodilated to different extents, giving rise to three different reference configurations and three different opening angles. Furthermore, we assume that the three deformed configurations share common values for B and C. The perfusion pressure $P = 100$ mmHg is uniform across all experiments, so given B, C and the three angles $\Theta_{0,C}$, $\Theta_{0,L}$ and $\Theta_{0,A}$, we could solve

$$(c_k)^2 - (b_k)^2 - \frac{\Theta_{0,k}}{\pi\Lambda}(C^2 - B^2) = 0,$$
$$-\frac{P\Theta_{0,k}\Lambda}{\pi} + \int_B^C H[\alpha(R')]\frac{\mathrm{d}R'}{R'} = 0,$$

for $k = C, L, A$ (6 equations in total) to find b_C, c_C, b_L, c_L, b_A and c_A, the vessel radii of control, ligated and anastomosed arteries. Experimentally, arteries are fixed by an agent such as formaldehyde after the animals are sacrificed, and the fixing pressure is not the same as the *in-vivo* pressure. Although we are calibrating using a fixing perfusion pressure instead of the *in-vivo* pressure, the perfusion pressure is usually chosen to be close to the *in-vivo* pressure so that vessel radii are not significantly affected.

If b_C, c_C, b_L, c_L, b_A, and c_A are unknown and B, C, $\Theta_{0,C}$, $\Theta_{0,L}$, and $\Theta_{0,A}$ are known, we write the forward problem as

$$(b_C, c_C, b_L, c_L, b_A, c_A) = \mathbf{f}(B, C, \Theta_{0,C}, \Theta_{0,L}, \Theta_{0,A}),$$

for a function $\mathbf{f} : \mathbb{R}^5 \mapsto \mathbb{R}^6$. However, in the flow alteration experiments, the deformed configuration is *observed* and the reference configuration is *unknown*. Defining $\omega_C = 2\pi - 2\Theta_{0,C}$, $\omega_L = 2\pi - 2\Theta_{0,L}$ and $\omega_A = 2\pi - 2\Theta_{0,A}$, we have 5 parameters to determine: B, C, ω_C, ω_L and ω_A. We choose them to minimize the sum of squared relative errors

$$R_1 = \sum_{k=C,L,A} \left\{ \left(\frac{b_k - b_{k,data}}{b_{k,data}} \right)^2 + \left(\frac{M_k - M_{k,data}}{M_{k,data}} \right)^2 \right\}, \tag{70}$$

where $M_k = \pi({c_k}^2 - {b_k}^2)$, and $b_{k,data}$ and $M_{k,data}$ are the lumen radii and medial CSAs taken from Table 2. This optimization procedure yields global shape parameters for the arteries in the reference state:

$$\begin{aligned} B &= 0.91 \text{ mm} && (71)\\ C &= 1.06 \text{ mm} && (72)\\ \omega_C &= 149^\circ && (73)\\ \omega_L &= 180^\circ && (74)\\ \omega_A &= 144^\circ. && (75) \end{aligned}$$

In particular, we predict that $\omega_A < \omega_C < \omega_L$ indicating that SMCs are more contracted in ligated arteries and more relaxed in anastomosed arteries, compared to controls. The model outputs for lumen radii and media cross sectional area, together with experimentally measured values are summarized in Fig. 5. The numerical values for the arterial radii and cross-sectional areas under a perfusion pressure of $P = 100$ mmHg are given in Table 3. The theoretical lumen radii b_C, b_L, b_A and medial cross-sectional areas M_C, M_L, M_A match the experimental values $b_{C,data}$, $b_{L,data}$, $b_{A,data}$ and $M_{C,data}$, $M_{L,data}$, $M_{A,data}$ well with a maximum relative error of about 6%. When the pressure is reduced to $P = 91$ mmHg (an estimated *in-vivo* lumen pressure) and b, c are recomputed from (45)-(46), the *in-vivo* radii differ from the radii of vessels under a $P = 100$ mmHg perfusion pressure by less than 1%.

3.1.2 Inferring Nitric Oxide Adaptation Parameters

We now turn our attention to the flow rate data in Table 2, taken from Lee and Langille (1991) and Langille et al. (1989). With this hemodynamic data, we calibrate the vasodilation component of our model.

In our calibration, some parameters are inferred from fitting to data while others are independently estimated. Table 4 summarizes both types of parameter. Recall that U from eq. (42) is the level of NO required to achieve 50% activation in terms of opening angle. Chen et al. (2008) report a wide range of values for U, ranging from 3 – 1600 nM. The value we adopt of $U = 300$ nM $= 3{\times}10^{-13}$ mol/mm^3 is the mean value from Table 2 of their paper.

Simulated control artery	Simulated ligated artery	Simulated anastomosed artery
$b_C = 0.87$ mm	$b_L = 0.73$ mm	$b_A = 0.90$ mm
$c_C = 0.93$ mm	$c_L = 0.79$ mm	$c_A = 0.96$ mm
$M_C = 0.35$ mm^2	$M_L = 0.30$ mm^2	$M_A = 0.36$ mm^2

Table 3: Predicted, simulated vessel dimensions (under perfusion pressure $P = 100$ mmHg) after calibrating against data in Table 2. With optimally chosen parameters in (71)-(75), lumen radii b_C, b_L, b_A are well-matched with $b_{C,data}$, $b_{L,data}$ and $b_{A,data}$ from Table 2 and similarly with medial cross-sectional areas $M_i = \pi(c_i^2 - b_i^2)$ for $i = C, L, A$.

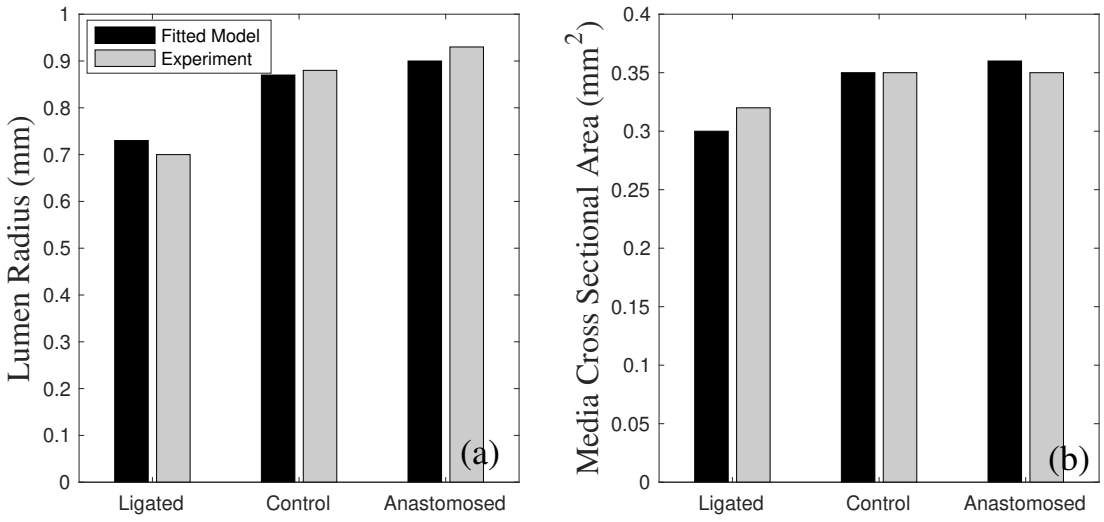

Figure 5: Lumen radii and Media Cross Sectional Areas (CSAs) for calibrated model. Reference radii B, C and opening angles ω_C, ω_L and ω_A were chosen (see eqs. (71)-(75)) so that lumen radii and media CSAs matched experimental values as closely as possible.

Symbol	Meaning	Value	Method of Estimation:
U	Parameter in OA-NO dose response: see eq. (42)	3×10^{-13} mol/mm^3	Mean value from Chen et al. (2008)
q_{ref}	Reference value for NO production rate	5×10^{-14} mol/mm^2/s	From Vaughn et al. (1998)
B	Inner radius of reference artery	0.91 mm	Fitted to data
C	Outer radius of reference artery	1.06 mm	Fitted to data
M	Hill coefficient in OA-NO dose response	2	Model choice
μ	Dynamic viscosity of blood	3×10^{-3} Pa s	O'Brien et al. (2011)
D_{NO}	Diffusivity of NO	3.4×10^{-3} mm^2/s	Lancaster (1994)
k	Decay rate of NO	0.17/s	Estimated from half-life
Λ	Axial Stretch	1.6	From Doyle and Dobrin (1971)
$\omega_{\max}$	Maximum OA	220°	From Williams et al. (2009)
$\omega_{\min}$	Minimumm OA	0°	Model choice
p_1	Parameter in NO-WSS dose response	0.00	Fitted to data
p_2	Parameter in NO-WSS dose response	0.20	Fitted to data
p_3	Parameter in NO-WSS dose response	0.047 Pa^{-2}	Fitted to data

Table 4: Global parameters in vasodilation model. "Fitted to data" indicates the values were found from calibrating the model: see sections 3.1.1 and 3.1.2. Abbreviations: OA = Opening Angle, WSS = Wall Shear Stress, NO = Nitric Oxide.

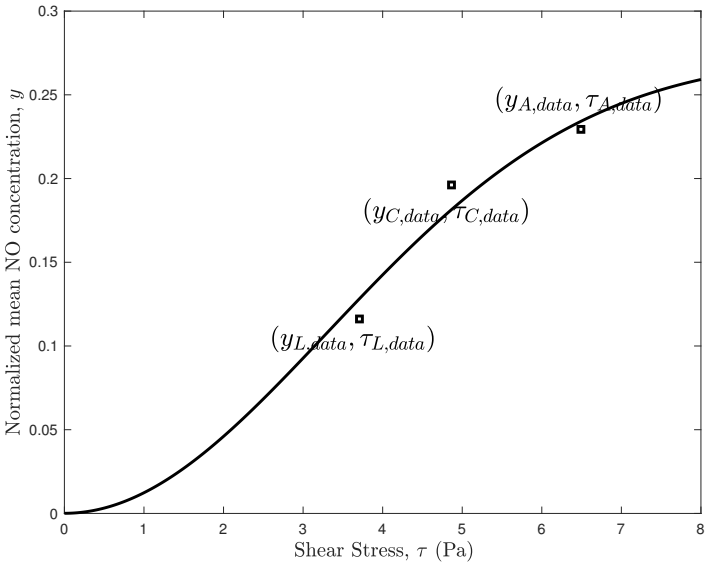

Figure 6: Normalized average NO concentration as a function of endothelial shear stress, along with best-fit sigmoidal curve $f(\tau) = p_1 + p_2(1 - e^{-p_3\tau^2})$. The quantities y_L, y_C and y_A are related to estimated NO levels in ligated, control and anastomosed rabbit carotid arteries respectively through eq. (78). Best-fit parameters are $p_1 = 0.00$, $p_2 = 0.20$, $p_3 = 0.047$ Pa^{-2}.

As discussed after eq. (39), the reference value for NO release rate q_{ref} was computed by Vaughn et al. (1998). The reference radii B and C were found from section 3.1.1 and we set $M = 2$. The values of blood viscosity μ, and diffusivity of nitric oxide D_{NO} are well documented in O'Brien et al. (2011) and Lancaster (1994). The decay rate of nitric oxide k was computed by assuming the half-life of the radical to be 4 seconds. Finally, we estimate $\Lambda = 1.6$, the axial pre-stretch, from experiments on dog carotid arteries (Doyle and Dobrin, 1971).

Unfortunately, we could not find experiments that measured opening angle as a function of NO concentration in rabbit carotid arteries, although Najibi and Cohen (1995) report *tone* as a function of NO concentration. The lack of this data means our estimates of $\omega_{\max}$ and $\omega_{\min}$ in eq. (42) will be imprecise. Williams et al. (2009) report an opening angle for rabbit carotids of about 220°: in Fig. 4 of their paper, they found that $\omega/2 \sim 108°$. Assuming that the treated arteries do not contain significant amounts of NO when the opening angle was measured, we take $u = 0$ throughout the section implying that $\omega_{\max} = 220°$. In the absence of further data, we also take $\omega_{\min} = 0°$, corresponding to a fully relaxed state with no residual stress when NO is in excess throughout the arterial wall.

Eq. (41) gives the shear stress on the endothelium and eq. (42) with $M = 2$ relates the mean NO concentration in the vessel wall to the opening angle:

$$\tau_{k,data} = \frac{4\mu Q_{k,data}}{\pi {b_{k,data}}^3}, \qquad \langle u_k \rangle = U\sqrt{\frac{\omega_{\max} - \omega_k}{\omega_k - \omega_{\min}}}, \tag{76}$$

	Control	Ligated	Anastomosed
Opening angle	$\omega_C = 149^\circ$	$\omega_L = 180^\circ$	$\omega_A = 144^\circ$
Shear stress (Pa)	$\tau_{C,data} = 4.87$	$\tau_{L,data} = 3.71$	$\tau_{A,data} = 6.49$
Mean NO conc. ($\times 10^{-13}$ mol/mm^3)	$\langle u_C \rangle = 2.1$	$\langle u_L \rangle = 1.4$	$\langle u_A \rangle = 2.2$

Table 5: Predicted morphological and biomechanical properties of control, ligated and anastomosed vessels.

for $k = C, L, A$. Values of ω_k were established in the previous section: see eqs. (73)-(75). A summary of shear stresses $\tau_{k,data}$, NO concentrations $\langle u_k \rangle$ and opening angles ω_k derived from experimental data is given in Table 5. Defining

$$y = \frac{\langle u \rangle \lambda D_{NO} K_1(\lambda b)(c^2 - b^2)}{2q_{\text{ref}} \int_b^c r K_0(\lambda r) dr}, \tag{77}$$

and

$$y_{k,data} = \frac{\langle u_k \rangle \lambda D_{NO} K_1(\lambda b_{k,data})(c_k{}^2 - b_{k,data}{}^2)}{2q_{\text{ref}} \int_{b_{k,data}}^{c_k} r K_0(\lambda r) dr}, \tag{78}$$

eq. (44) becomes

$$f(\tau) = p_1 + p_2(1 - \exp(-p_3 \tau^2)) = y. \tag{79}$$

Therefore, given the data $((\tau_{C,data}, y_{C,data}), (\tau_{L,data}, y_{L,data}), (\tau_{A,data}, y_{A,data}))$, we must find best-fit parameters p_1, p_2, p_3 such that (79) is satisfied in the least squares sense (i.e. $\sum_{k=C,L,A} [f(\tau_{k,data}; p_1, p_2, p_3) - y_{k,data}]^2$ is minimized). While values of c_k were calculated in the first calibration step (see Table 3), in (78) we use actual data for vessel radii whenever it is available (i.e. the formula (78) involves $b_{k,data}$ rather than b_k).

We find that the best-fit parameters for $f(\tau)$ are

$$p_1 = 0.00, \quad p_2 = 0.20, \quad p_3 = 0.047 \text{ Pa}^{-2}, \tag{80}$$

see Fig. 6 which shows the optimized dose-response curve for NO release rate as a function of shear stress for endothelial cells from rabbit carotids. Humphrey (2008) has published similar data from bovine aortic endothelial cells. Quantitatively, our results are different with saturation occurring much more slowly with respect to shear stress. Another difference is that our mean NO concentration is effectively zero at $\tau = 0$ whereas data from Humphrey (2008) suggests $p_1 > 0$. Figure 6 shows that shear stress needs to exceed ~ 8 Pa for maximal NO release, whereas the corresponding value for bovine endothelial cells is about 0.6 Pa. We expect the curves to differ not only because the animal models are different (bovine aorta vs. rabbit carotid), but also because Humphrey (2008) uses NO synthase mRNA as the experimental proxy for NO release, rather than NO concentration, which would be challenging to measure directly.

With the values from Table 4, we now solve eqs. (45)-(49) numerically with $g(Q, t) = 1$: see Figure 7. The main take-away is that larger values of NO flux q_{ref} result in more strongly

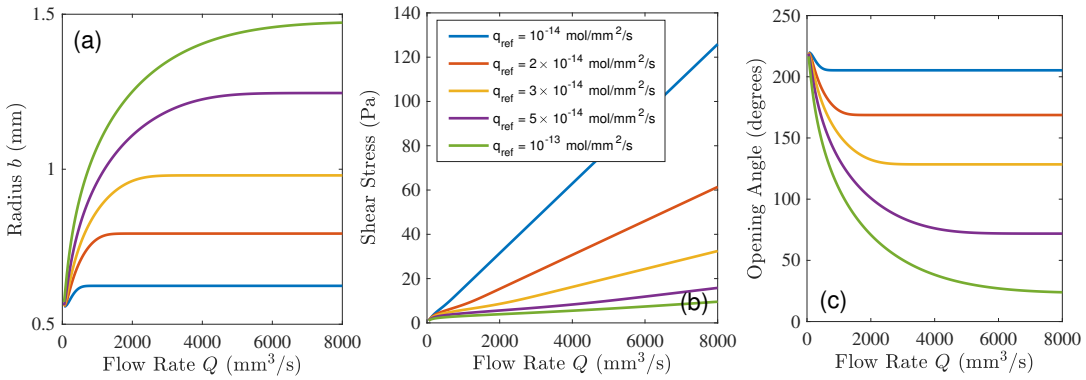

Figure 7: Evolution of lumen radius, shear stress and opening angle with respect to flow rate Q. Parameters were $B = 0.91$ mm, $C = 1.06$ mm, $\omega_{\min} = 0$, $\omega_{\max} = 220°$, $(p_1, p_2, p_3) = (0, 0.20, 0.047\ \text{Pa}^{-2})$.

regulated shear stresses. Values of shear stress are kept low providing the opening angle is able to continually decrease with respect to flow rate Q (Fig. 7(c)). When the opening angle reaches its lower bound and saturates, the radius also saturates (Fig. 7(a)): the artery has dilated to its maximum capacity and further increases in flow rate do not significantly change the arterial dimensions. The result is that while the NO release mechanism is able to keep shear stresses low for small flow rates, the vessel falls into the "no regulation" case of Fig. 1 for extremely large flow rates.

In Figure 8, we calculate hoop and radial stress distributions at different flow rates. Fig. 8(a) shows that the Cauchy hoop stress is dominant and tensile, whereas the radial stress is compressive: this is in-line with predictions from classical biomechanical theory: see for example Fig. 7.35 in Humphrey (2013). Recall that the residual stress in a body is the stress that remains after all external forces (in our case the lumen pressure, P) have been removed. As the flow rate increases, more NO is released into the media and there is a relaxation of this layer manifested as a reduction in magnitude of the residual hoop and radial stresses in Fig. 8(b) and a decrease in opening angle in Fig. 8(c).

While unloaded arteries with a larger flow rate Q have higher levels of NO and are more dilated in 8(b), it is interesting that *pressurized* vessels experience greater tension with respect to Q in Fig. 8(a). In Fig. 8(b), the vessels have approximately the same wall thickness but different lumen sizes. However, when subjected to the same pressure, arteries with larger lumens – but identical wall thickness – undergo a larger strain. (To understand this, note that an artery with a larger lumen has a smaller wall thickness relative to its lumen radius. Given two annuli with the same inner radius but different wall thicknesses, the thinner annulus will undergo greater dilation under the same pressure.) Therefore, arteries subjected to a larger flow rate also manifest a greater circumferential stress in Fig. 8(a).

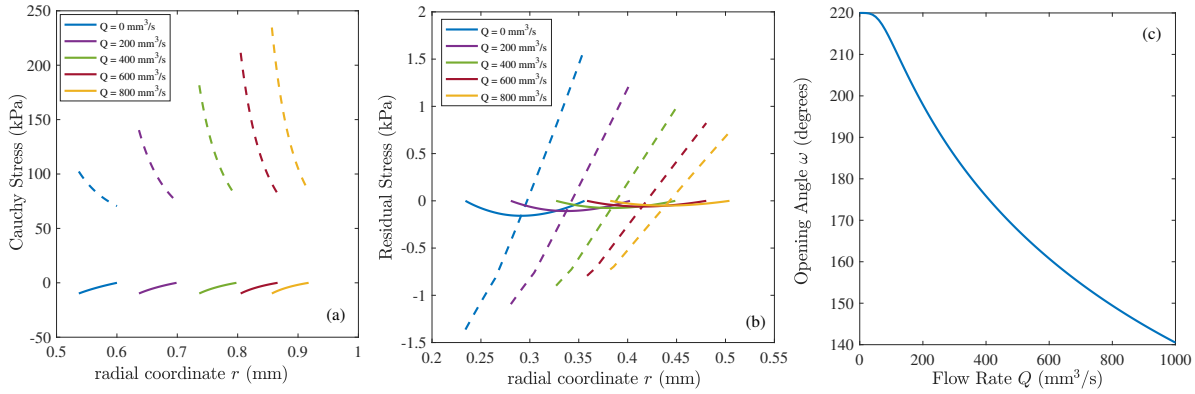

Figure 8: Evolution of Cauchy and residual stresses for increasing flow rate Q in the case of pure vasodilation. (a) Cauchy hoop stresses increase with Q while (b) residual stresses decrease. (c) Opening angle as a function of flow rate. Dashed curves indicate hoop stresses while solid curves indicate radial stresses. Parameters were $P = 73.6$ mmHg, $B = 0.91$ mm, $C = 1.06$ mm, $q_{\text{ref}} = 5 \times 10^{-14}$ mol/mm^2/s.

3.2 Pure Growth in L-NAME treated Weanling Arteries

We now consider the case of pure growth, without any vasodilation. As well as taking morphological measurements, Tronc et al. (1996) counted the number of smooth muscle cells in the media for control and L-NAME treated rabbits: see the final rows in Tables 6 and 7. We can use this data to infer a hypothetical growth function for the experiments. The SMC measurements define the growth Jacobian in the media:

$$J_g(Q) = \det \mathbf{F}_g = g^2 = \frac{N(Q)}{N_0}, \tag{81}$$

where N_0 is the number of SMCs without the fistula (2062 and 1773 for control and L-NAME treated arteries respectively) and $N(Q)$ is the number of SMCs when the flow rate is increased to Q by the fistula. From eq. (69)

$$\begin{aligned} J_g(Q) &= g^2 = \left\{ \left(\frac{Q}{Q_0}\right)^{1/3} + \left(1 - \left(\frac{Q}{Q_0}\right)^{1/3}\right) e^{-t/T} \right\}^2, \\ &= (c_1 Q^{1/3} + c_2)^2, \end{aligned}$$

where $c_1 = Q_0^{-1/3}(1 - e^{-t/T})$, $c_2 = e^{-t/T}$. In the control arteries of Table 6, we have $J_g(490) = 1$, $J_g(3270) = 2.18$, so solving for c_1 and c_2 yields $c_1 = 0.068$, $c_2 = 0.460$ and we have

$$\begin{aligned} Q_0 &= 490 \text{ mm}^3/s, \\ t/T &= 0.77. \end{aligned}$$

Quantity	Without Fistula	With Fistula (increased flow)
Perfusion Pressure	$P = 73.6$ mmHg	$P = 73.6$ mmHg
Flow Rate	$Q_1 = 490$ mm^3/s	$Q_2 = 3270$ mm^3/s
Wall Shear Stress	$\tau_1 = 1.07$ Pa	$\tau_2 = 0.887$ Pa
Lumen Radius,	$b_1 = 1.27$ mm	$b_2 = 2.32$ mm
Media Cross Sectional Area, M	$M_1 = 0.36$ mm^2	$M_2 = 0.75$ mm^2
# Smooth Muscle Cells in Media	2062	4504

Table 6: Hemodynamic data for control arteries from Tronc et al. (1996).

Quantity	Without Fistula	With Fistula (increased flow)
Perfusion Pressure	$P = 73.6$ mmHg	$P = 73.6$ mmHg
Flow Rate Q	$Q_3 = 558$ mm^3/s	$Q_4 = 1768$ mm^3/s
Wall Shear Stress	$\tau_3 = 1.91$ Pa	$\tau_4 = 1.87$ Pa
Lumen Radius	$b_3 = 1.075$ mm	$b_4 = 1.62$ mm
Media Cross Sectional Area	$M_3 = 0.26$ mm^2	$M_4 = 0.49$ mm^2
# Smooth Muscle Cells in Media	1773	2717

Table 7: Hemodynamic data for L-NAME treated arteries from Tronc et al. (1996).

Administration of L-NAME suppresses NO but is not supposed to affect growth. This is confirmed by repeating the calculation for the L-NAME treated arteries. From Table 7, we have $J_g(558) = 1$, $J_g(1768) = 1.53$ yielding $(c_1, c_2) = (0.061, 0.495)$ and $Q_0 = 558\text{mm}^3/s$ and $t/T = 0.71$. There is not a large change in either Q_0 or t/T for the L-NAME treated rabbits: administration of L-NAME did not significantly impact the growth function. Since $t/T < 1$ for both sets of rabbits, we hypothesize that the arteries in these animals have not fully adapted to their altered hemodynamical environment. Interestingly, the flow alteration experiments by Tronc et al. (1996) were only performed for 1 month, in contrast to the experiments in Fig. 1 which lasted up to 6-8 months.

To test our hypothesis, in Figure 9, we reproduce the lumen radii and shear stresses from Tronc et al. (1996) for the arteries of NO-inhibited weanling rabbits. The data is very noisy but seem to suggest that under various flow rates, the lumen radius stays approximately constant as growth proceeds. The shear stress exhibits approximately linear behavior, confirming that the arteries in Tronc et al. (1996) are still in the early stages of their adaptation.

Having calculated reference shear stress values of $Q_0 \approx 490$ mm^3/s and $Q_0 \approx 558$ mm^3/s from SMC numbers, we now assume a reference flow rate of $Q_0 = 500$ mm^3/s for the growth law in (69). By taking the NO concentration $u = 0$ throughout the artery, we have $\omega = \omega_{\max}$ and SMCs are always in their maximally contracted state. Our model consists of eqs. (45), (46), (49) and (69). We solve these equations numerically using Matlab's `fsolve` for b, c and τ for different values of t/T. In Figure 10, we see that at early times, there is no shear stress regulation: the radius b remains constant with respect to Q while the shear stress increases linearly with Q. At later times, we have more regulation: for $t/T = 5$ the radius exhibits the

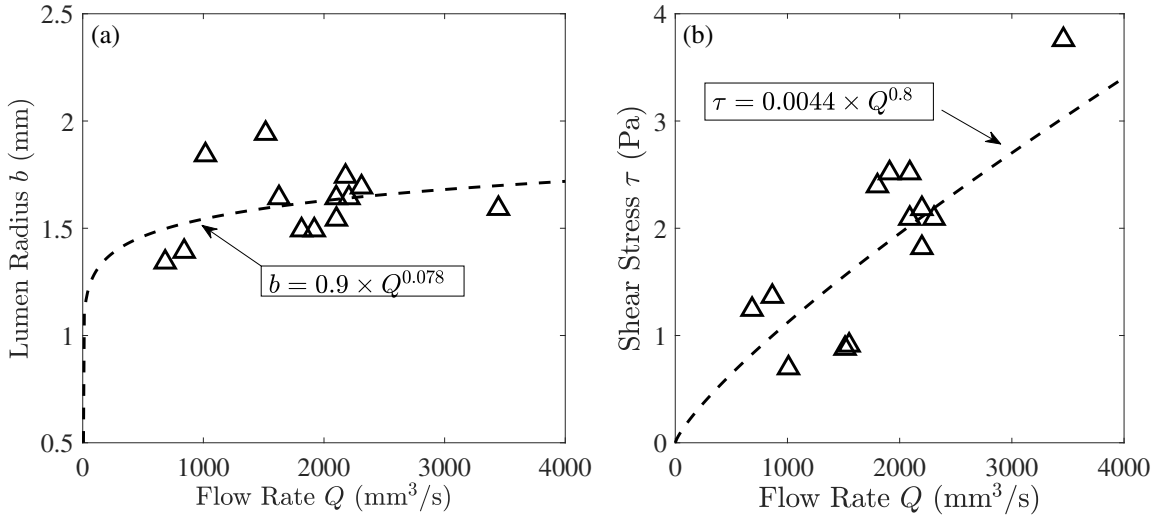

Figure 9: Data from weanling rabbits treated with L-NAME. (a) Lumen radius is approximately constant with respect to flow rate; dashed line is the best-fit curve of the form $b = \kappa Q^a$ yielding $\kappa = 0.9$, $a = 0.078$. (b) Shear stress is approximately linear with flow rate; dashed line is the best-fit curve of the form $\tau = \kappa Q^a$ yielding $\kappa = 0.0044$, $a = 0.8$. Data (black triangles) is taken from Tronc et al. (1996). The data suggests that very little shear stress regulation is occurring, or that not enough time has elapsed in the experiment for regulation to occur.

characteristic $Q^{1/3}$ scaling whereas the shear stress remains essentially constant with respect to Q. However, the predicted homeostatic value of ~ 10 Pa (green curve) is on the large side: NO-regulated carotid arteries under normal flow conditions exhibit a shear stress of about 1-5 Pa irrespective of whether growth occurs (Tronc et al., 1996) or not (Lee and Langille, 1991). Our model can reproduce a lower shear stress when the opening angle is fixed to a lower value (e.g. $\omega = \pi/2$ instead of $\omega_{\max}$). In section 3.3, we will see how the presence of NO in growing arteries decreases ω and subsequently lowers the homeostatic shear stress.

Finally, in Figure 11 we explore how radial and hoop stresses change as growth occurs. We see that stress profiles are carried materially by the arterial wall with minimum and maximum values remaining unaltered. The only distortion of the stress distribution arises from growth and deformation of the domain $b < r < c$. Mathematically, the radial and hoop stresses are functions of R: $T_{rr} = T_{rr}(R)$ and $T_{\theta\theta} = T_{\theta\theta}(R)$ (shown in Figure 11(c) as solid and dashed curves respectively). These functions are independent of g, and therefore also independent of Q and t, consistent with the calculations in Lemma 1. In our single layer model, when growth is isotropic in the radial and circumferential directions and constant with respect to position, the strains in the artery (in particular the circumferential strain α) are unaltered by growth, so we would not expect changes in the stress profiles either.

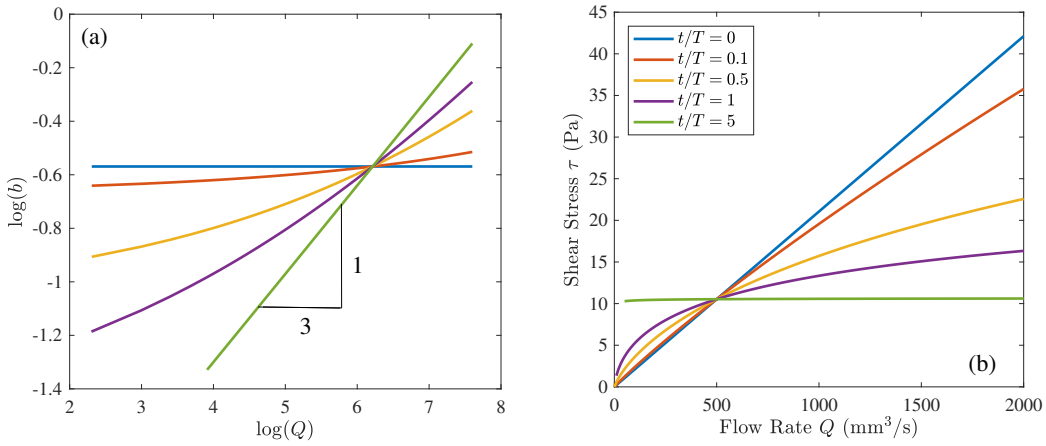

Figure 10: Predicted radii (a) and shear stresses (b) as a function of flow rate, in the case of pure growth. Reference radii $B = 0.9$ mm, $C = 1.0$ mm, axial stretch $\Lambda = 1.6$, lumen pressure $P = 100$ mmHg and opening angle $\omega = \omega_{\max} = 220°$ using the growth function (69) with $Q_0 = 500$ cm^3/s.

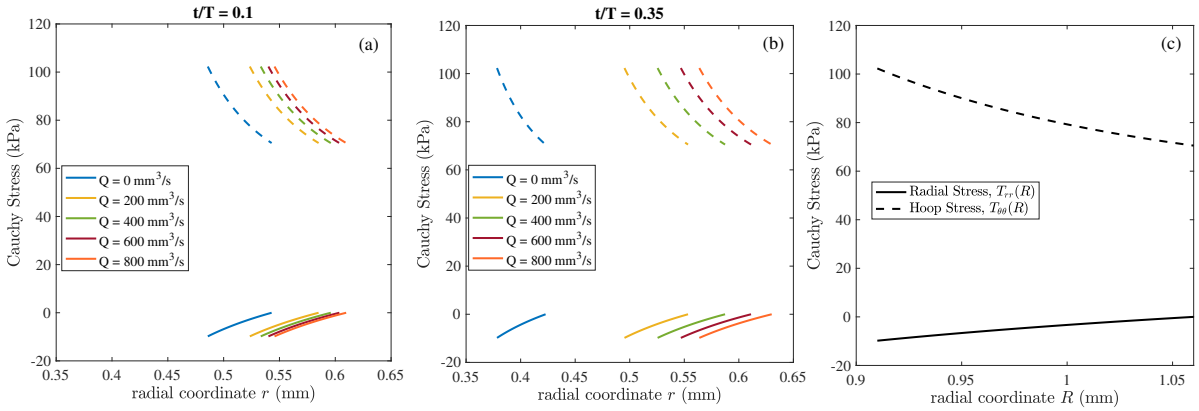

Figure 11: Cauchy stresses for different flow rates in the pure growth regime. (a) $t/T = 0.1$ (b) $t/T = 0.35$. Stresses are materially advected with the arterial wall. (c) When plotted as a function of the reference radius R stress distributions are invariant with respect to Q and t/T. Dashed and solid curves represent hoop and radial stresses respectively. Parameters were $P = 73.6$ mmHg, $B = 0.91$ mm, $C = 1.06$ mm, $Q_0 = 500$ mm^3/s.

3.3 Growth and Vasodilation in Weanling Arteries

We now study the final case where both growth and vasodilation play a role in deforming the artery. The governing equations are (45)-(49) supplemented with the growth law (69) and we assume $Q_0 = 500$ mm^3/s. Our results for shear stress regulation are shown in Fig. 12. It is instructive to compare this figure with the pure growth case, Fig. 10.

In the pure growth case, the opening angle was always saturated at its maximum value $\omega = \omega_{\max}$. The complete absence of NO essentially made the artery stiffer with the consequence that radii were smaller and shear stresses were larger. In Fig. 12, we see that when ω is allowed to float, the vessel is more relaxed and compliant. Dilation requires less energy, radii are larger, and shear stresses are smaller compared to the pure growth case. Vasodilation is most effective at reducing shear stress at small times: even when t/T is small and there has not been sufficient time for growth, we see that shear stresses are kept below about 6.5 Pa when $0 \leq Q \leq 2000$ mm^3/s. In contrast, Fig. 10 has shear stresses shooting up to 35 Pa at $Q = 2000$ mm^3/s for $t/T = 0.1$. In both Figures 10 and 12, when t/T is larger, shear stresses are kept almost constant. But in Figure 12 when both NO release and growth can function in concert, the constant is lowered to a value that is much more in-line with experiments. For a fully-adapted artery, we predict a homeostatic shear stress of ≈ 3.8 Pa and the model selects an opening angle $\omega \approx 170^\circ$ over a range of flow rates (green curves in Fig. 12).

Again, we can provide some qualitative confirmation of these hypotheses by examining the data from experiments. In Fig. 13, we find the best-fit q_{ref} and t/T to minimize the sum of squared relative errors between model and experimental radii. While 8 data points are available for the radius as a function of flow rate in Tronc et al. (1996), only two values of media CSA were published (the values are reproduced in Table 6). Reference radii were fixed at $B = 1.1$ mm and $C = 1.2$ mm. Once $b(Q)$ is found from this procedure, the shear stress $\tau(Q)$ is calculated from eq. (49). The optimization gives $q_{\text{ref}} = 4.4 \times 10^{-12}$ mol/mm^2/s and $t/T = 0.45$, again suggesting that there is only partial regulation through growth. A comparison of Fig. 13 with Fig. 9 shows that vasodilation helps to suppress shear stress as flow rate increases: recall the only difference between the two figures is that the data from Fig. 9 is from L-NAME treated weanling rabbits while the data from Fig. 13 is from untreated weanling rabbits. Both sets of rabbits have arterial media that grow, but the first set of rabbits have arteries that have inhibited NO. Figure 13(a) shows a clear increase in radius with flow rate and, with the exception of a single data point near $Q = 6000$ mm^3/s, a concomitant suppression of shear stress. The occurence of this outlier was probably due to the artery developing pathologies that interfered with its adaptation, or being unable to grow to its target size within the duration of the experiment.

In Figure 14 we study the stress distributions for a growing, vasodilating artery. The results combine our observations from Figs. 8 and 11. We see that the Cauchy hoop stress is dominant, increases with flow rate and converges to an asymptotic distribution as $Q \to \infty$. Recall that the residual stress is defined as the stress remaining in the body after all external forces have been removed. The only external force in our model is the lumen pressure P, so the residual hoop stress, for example, is calculated by taking $P = 0$ in eq. (36). The magnitude of the residual hoop and radial stresses decrease with flow rate and the radial

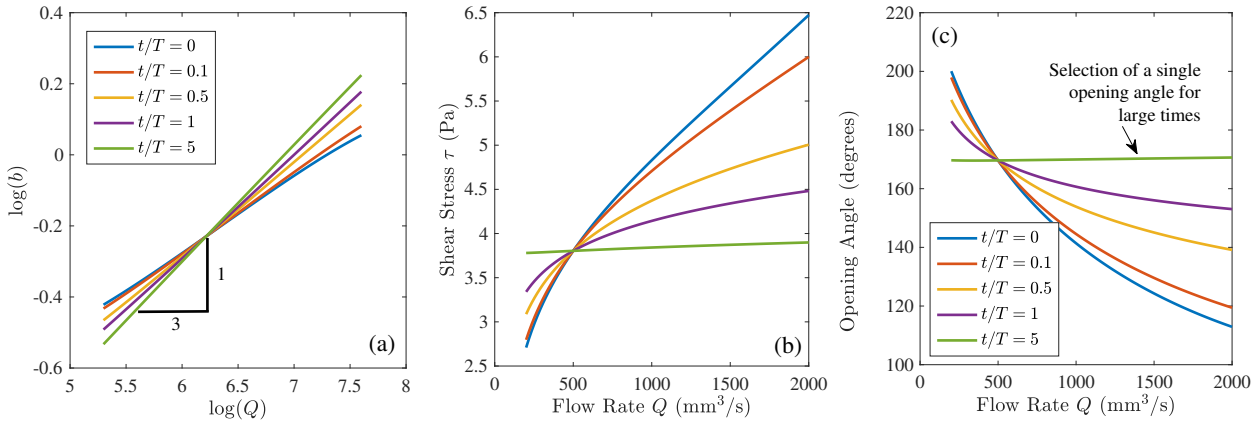

Figure 12: The joint effects of growth and vasodilation on radius, shear stress, and opening angle. Parameters were $P = 100$ mmHg, $B = 0.9$ mm, $C = 1.0$ mm, $q_{\text{ref}} = 5 \times 10^{-14}$ mol/mm^2/s, $Q_0 = 500$ mm^3/s.

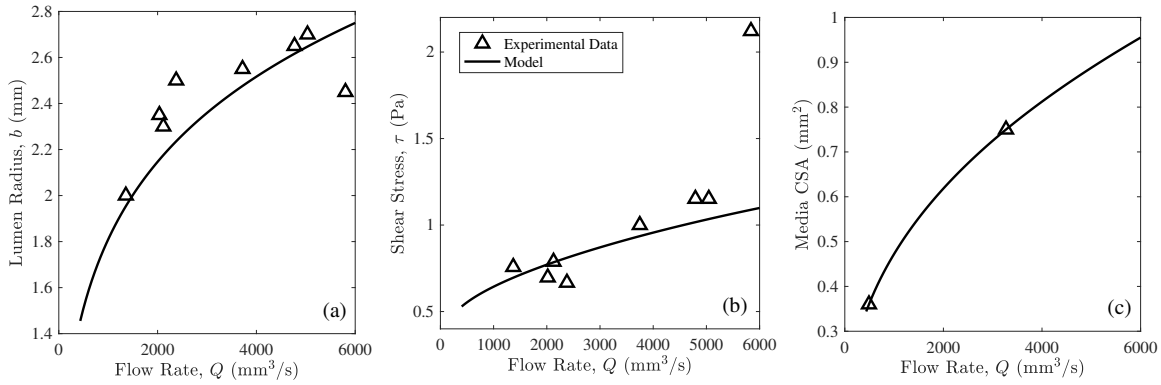

Figure 13: Comparison of joint vasodilation-growth model with morphological data from weanling rabbits (Tronc et al., 1996). Parameters were $P = 73.6$ mmHg, $B = 1.1$ mm, $C = 1.2$ mm, $t/T = 0.45$ and $q_{\text{ref}} = 4.4 \times 10^{-12}$ mol/mm^2/s, $Q_0 = 500$ mm^3/s.

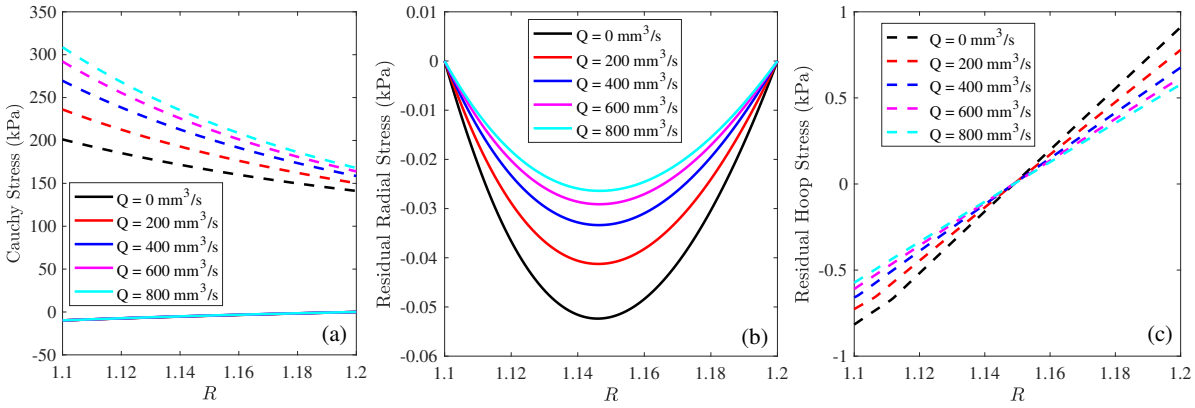

Figure 14: Evolution of Cauchy and residual stress distributions with flow rate Q for the case of joint growth and vasodilation. Dashed (solid) lines indicate hoop (radial) stresses. (a) Cauchy hoop stress increases as flow rate increases. (b) Residual radial stress decreases in magnitude as Q increases. (c) Residual hoop stress can be tensile or compressive and decreases in magnitude as Q increases. Parameters were $B = 1.1$ mm, $C = 1.2$ mm, $q_{\text{ref}} = 5 \times 10^{-14}$ mol/mm^2/s and $Q_0 = 500$ mm^3/s. $P = 73.6$ mmHg in (a) and $P = 0$ mmHg in (b,c).

residual stress is zero at the inner and outer boundaries of the media because both boundaries are traction-free. Unlike the pure growth case Fig. 11, the radial and hoop stresses do not collapse onto a single "universal" curve when plotted as a function of the reference radial coordinate R.

4 Conclusion

In this paper, we proposed a theoretical model to describe how an arterial section adapts to its hemodynamic environment based on nitric oxide (NO) and PDGF release. The adaptation occurs through two mechanisms: a change in opening angle (and therefore residual stress) representing vasodilation; and a thickening of the media representing growth.

We explored the coupling of these phenomena by studying the model in cases of pure vasodilation, pure growth, and joint vasodilation and growth. We found that both vasodilation and growth contribute to shear stress regulation in complementary ways. Morphological changes in the vessel wall due to NO occur over short time scales while growth-induced adaptation of the artery proceeds more slowly, over much longer time scales. Both of these mechanisms help the vessel adapt to keep shear stress constant. Through our model, we can explain shear stress homeostasis in terms of dynamically evolving NO concentration, arterial opening angle, and wall thickness; as well as the static mechanical properties of the media – all of which are experimentally accessible quantities. Our most important results are Figures 10 and 12 which show the absence (presence) of regulation at early (late) times,

the importance of the opening angle in determining the homeostatic shear stress, and the function of NO in generally keeping the shear stress within a narrow range.

Our model generally reproduces the results from flow-alteration experiments on rabbit and canine carotid arteries. In particular, for a flow rate Q, it predicts a $Q^{1/3}$ scaling for the lumen radius for long times, resulting in the shear stress remaining *constant* with respect to Q as the arterial lumen expands. The result is exact for the case of pure growth (Fig. 10) and approximate when both vasodilation and growth are present (Fig. 12). When arteries are subjected to increased flow for only a short time, they can vasodilate to reduce shear stress (Fig. 13). However, when their capacity to dilate is reduced through NO inhibition, shear stress rapidly increases with flow rate (Fig. 9).

Although our model has explained and integrated many types of flow-alteration experiments, it also has several deficiencies. First, we have neglected changes in the composition in the media as remodeling occurs. In this respect, mixture models developed by authors such as Karšaj and Humphrey (2012) still provide the gold standard. Second, our results assume that the artery consists of a single layer (the media) and ignores the adventitia. Including an NO-dependent opening angle for a two-layer model would be challenging because the opening angles for the media and adventitia are different. Note also that the results of Lemma 1 would no longer hold with the addition of a second mechanically significant layer. Third, although we calibrated our model with data in the form of lumen radii and media cross-sectional areas for different flow rates, the experiments that we surveyed did not monitor the opening angle. Knowledge of the opening angle would yield more accurate values for $\omega_{\min}$ and $\omega_{\max}$ and a better representation of the stress-free state. Fourth, the "no-bending" assumption in section 2 is a strong one: in practice, the reference radii B and C in Fig. 3 could change with opening angle. Inferring the geometry of an underlying stress-free reference configuration as an artery grows, adapts, and remodels, still poses a significant challenge for theorists. Finally, our modeling of PDGF-induced growth is overly simple. We captured its effect through an algebraic relationship between the flow rate and the growth tensor, ignoring its transport (Fok and Sanft, 2017), production (Irons and Humphrey, 2020) and interactions with other signaling agents (Yu et al., 2012).

In summary, we have presented a 2D biomechanical arterial model that is capable of reproducing the morphological results from a wide range of flow-alteration experiments in carotid arteries. This model could be used as a building block to describe more complicated phenomena such as flow impairment in media sclerosis (Lanzer et al., 2021), chronic inward remodeling in atherosclerosis (Glagov et al., 1987), or tissue remodeling in hypertension (Rizzoni et al., 1996).

5 Declarations.

All data generated or analysed during this study are included in this published article. The author has no relevant financial or non-financial interests to disclose. No funding was received to assist with the preparation of this manuscript.

References

P. W. Alford, J. D. Humphrey, and L. A. Taber. Growth and remodeling in a thick-walled artery model: effects of spatial variations in wall constituents. *Biomechanics and modeling in mechanobiology*, 7(4):245–262, 2008.

B. C. Berk, R. W. Alexander, T. A. Brock, M. A. Gimbrone Jr, and R. C. Webb. Vasoconstriction: a new activity for platelet-derived growth factor. *Science*, 232(4746):87–90, 1986.

K. Chen, R. N. Pittman, and A. S. Popel. Nitric oxide in the vasculature: where does it come from and where does it go? a quantitative perspective. *Antioxidants & redox signaling*, 10 (7):1185–1198, 2008.

R. H. Cox. Arterial wall mechanics and composition and the effects of smooth muscle activation. *American Journal of Physiology-Legacy Content*, 229(3):807–812, 1975.

P. F. Davies. Hemodynamic shear stress and the endothelium in cardiovascular pathophysiology. *Nature clinical practice Cardiovascular medicine*, 6(1):16–26, 2009.

J. C. de la Torre. Cerebral hemodynamics and vascular risk factors: setting the stage for alzheimer's disease. *Journal of Alzheimer's Disease*, 32(3):553–567, 2012.

J. Doyle and P. B. Dobrin. Finite deformation analysis of the relaxed and contracted dog carotid artery. *Microvascular research*, 3(4):400–415, 1971.

P.-W. Fok and R. Sanft. A biochemical and mechanical model of injury-induced intimal thickening. *Mathematical medicine and biology: a journal of the IMA*, 34(1):77–108, 2017.

S. Glagov, E. Weisenberg, C. K. Zarins, R. Stankunavicius, and G. J. Kolettis. Compensatory enlargement of human atherosclerotic coronary arteries. *New England Journal of Medicine*, 316(22):1371–1375, 1987.

R. Gleason, L. Taber, and J. Humphrey. A 2-d model of flow-induced alterations in the geometry, structure, and properties of carotid arteries. *J. Biomech. Eng.*, 126(3):371–381, 2004.

A. Goriely. *The mathematics and mechanics of biological growth*, volume 45. Springer, 2017.

A. Harris, G. Guidoboni, J. C. Arciero, A. Amireskandari, L. A. Tobe, and B. A. Siesky. Ocular hemodynamics and glaucoma: the role of mathematical modeling. *European journal of ophthalmology*, 23(2):139–146, 2013.

G. A. Holzapfel, G. Sommer, C. T. Gasser, and P. Regitnig. Determination of layer-specific mechanical properties of human coronary arteries with nonatherosclerotic intimal thickening and related constitutive modeling. *American Journal of Physiology-Heart and Circulatory Physiology*, 289(5):H2048–H2058, 2005.

G. A. Holzapfel et al. Biomechanics of soft tissue. *The handbook of materials behavior models*, 3:1049–1063, 2001.

J. Humphrey. Vascular adaptation and mechanical homeostasis at tissue, cellular, and sub-cellular levels. *Cell biochemistry and biophysics*, 50(2):53–78, 2008.

J. D. Humphrey. *Cardiovascular solid mechanics: cells, tissues, and organs*. Springer Science & Business Media, 2013.

L. Irons and J. D. Humphrey. Cell signaling model for arterial mechanobiology. *PLoS computational biology*, 16(8):e1008161, 2020.

Z. S. Jackson, A. I. Gotlieb, and B. L. Langille. Wall tissue remodeling regulates longitudinal tension in arteries. *Circulation research*, 90(8):918–925, 2002.

A. Kamiya and T. Togawa. Adaptive regulation of wall shear stress to flow change in the canine carotid artery. *Am J Physiol*, 239(1):H14–H21, 1980.

I. Karšaj and J. D. Humphrey. A multilayered wall model of arterial growth and remodeling. *Mechanics of materials*, 44:110–119, 2012.

J. R. Lancaster. Simulation of the diffusion and reaction of endogenously produced nitric oxide. *Proceedings of the National Academy of Sciences*, 91(17):8137–8141, 1994.

B. L. Langille, M. P. Bendeck, and F. W. Keeley. Adaptations of carotid arteries of young and mature rabbits to reduced carotid blood flow. *American Journal of Physiology-Heart and Circulatory Physiology*, 256(4):H931–H939, 1989.

P. Lanzer, F. M. Hannan, J. D. Lanzer, J. Janzen, P. Raggi, D. Furniss, M. Schuchardt, R. Thakker, P.-W. Fok, J. Saez-Rodriguez, et al. Medial arterial calcification: Jacc state-of-the-art review. *Journal of the American College of Cardiology*, 78(11):1145–1165, 2021.

R. D. B. Lee and B. L. Langille. Arterial adaptations to altered blood flow. *Canadian journal of physiology and pharmacology*, 69(7):978–983, 1991.

S. E. Lindsey, J. T. Butcher, and H. C. Yalcin. Mechanical regulation of cardiac development. *Frontiers in physiology*, 5:318, 2014.

T. Matsumoto, M. Tsuchida, and M. Sato. Change in intramural strain distribution in rat aorta due to smooth muscle contraction and relaxation. *American Journal of Physiology-Heart and Circulatory Physiology*, 271(4):H1711–H1716, 1996.

S. J. Mousavi, S. Farzaneh, and S. Avril. Patient-specific predictions of aneurysm growth and remodeling in the ascending thoracic aorta using the homogenized constrained mixture model. *Biomechanics and modeling in mechanobiology*, 18(6):1895–1913, 2019.

S. Najibi and R. A. Cohen. Enhanced role of k+ channels in relaxations of hypercholesterolemic rabbit carotid artery to no. *American Journal of Physiology-Heart and Circulatory Physiology*, 269(3):H805–H811, 1995.

S. O'Brien, N. J. Kent, M. Lucitt, A. J. Ricco, C. McAtamney, D. Kenny, and G. Meade. Effective hydrodynamic shaping of sample streams in a microfluidic parallel-plate flow-assay device: matching whole blood dynamic viscosity. *IEEE transactions on biomedical engineering*, 59(2):374–382, 2011.

A. Rachev. Theoretical study of the effect of stress-dependent remodeling on arterial geometry under hypertensive conditions. *Journal of biomechanics*, 30(8):819–827, 1997.

A. Rachev and K. Hayashi. Theoretical study of the effects of vascular smooth muscle contraction on strain and stress distributions in arteries. *Annals of biomedical engineering*, 27(4):459–468, 1999.

J. K. Raines, M. Y. Jaffrin, and A. H. Shapiro. A computer simulation of arterial dynamics in the human leg. *Journal of biomechanics*, 7(1):77–91, 1974.

A. B. Ramachandra, J. D. Humphrey, and A. L. Marsden. Gradual loading ameliorates maladaptation in computational simulations of vein graft growth and remodelling. *Journal of The Royal Society Interface*, 14(130):20160995, 2017.

D. Rizzoni, E. Porteri, M. Castellano, G. Bettoni, M. L. Muiesan, P. Muiesan, S. M. Giulini, and E. Agabiti-Rosei. Vascular hypertrophy and remodeling in secondary hypertension. *Hypertension*, 28(5):785–790, 1996.

E. K. Rodriguez, A. Hoger, and A. D. McCulloch. Stress-dependent finite growth in soft elastic tissues. *Journal of biomechanics*, 27(4):455–467, 1994.

P. Struijk, P. Stewart, K. Fernando, V. Mathews, T. Loupas, E. Steegers, and J. Wladimiroff. Wall shear stress and related hemodynamic parameters in the fetal descending aorta derived from color doppler velocity profiles. *Ultrasound in medicine & biology*, 31(11):1441–1450, 2005.

F. Tronc, M. Wassef, B. Esposito, D. Henrion, S. Glagov, and A. Tedgui. Role of no in flow-induced remodeling of the rabbit common carotid artery. *Arteriosclerosis, thrombosis, and vascular biology*, 16(10):1256–1262, 1996.

A. Valentin and J. Humphrey. Evaluation of fundamental hypotheses underlying constrained mixture models of arterial growth and remodelling. *Philosophical Transactions of the Royal Society A: Mathematical, Physical and Engineering Sciences*, 367(1902):3585–3606, 2009.

M. W. Vaughn, L. Kuo, and J. C. Liao. Estimation of nitric oxide production and reaction-rates in tissue by use of a mathematical model. *American Journal of Physiology-Heart and Circulatory Physiology*, 274(6):H2163–H2176, 1998.

C. Williams, J. Liao, E. Joyce, B. Wang, J. Leach, M. Sacks, and J. Wong. Altered structural and mechanical properties in decellularized rabbit carotid arteries. *Acta biomaterialia*, 5 (4):993–1005, 2009.

J. Yu, Y. Zhang, X. Zhang, R. D. Rudic, P. M. Bauer, D. C. Altieri, and W. C. Sessa. Endothelium derived nitric oxide synthase negatively regulates the pdgf-survivin pathway during flow-dependent vascular remodeling. *PloS one*, 7(2):e31495, 2012.

A Intracellular-Extracellular NO Model

One possible way to extend eq. (37) to include dependence on intracellular NO, v, is through the system of partial differential equations

$$\begin{aligned}\frac{\partial u}{\partial t} &= D_{NO}\nabla^2 u - ku - \sigma u,\\ \frac{\partial v}{\partial t} &= \sigma u - \hat{k}v,\end{aligned}$$

where σ is the rate at which NO is internalized by smooth muscle cells and $\hat{k}$ is the degradation rate inside smooth muscle cells. Assuming $\sigma \ll k$, the equations at steady state become

$$\begin{aligned}D_{NO}\nabla^2 u - ku = 0,\\ v = \sigma u/\hat{k},\end{aligned} \tag{82}$$

and intracellular and extracellular NO are proportional to each other. If k and σ are comparable, or if $\sigma > k$, k in eq. (82) must be replaced by $k + \sigma$. If we postulate a Hill function relationship between the opening angle ω and intracellular NO concentration

$$\omega = \omega_{\max} - (\omega_{\max} - \omega_{\min})\frac{\langle v\rangle^M}{V^M + \langle v\rangle^M},$$

for some constant V, then

$$\begin{aligned}\omega &= \omega_{\max} - (\omega_{\max} - \omega_{\min})\frac{(\sigma/\hat{k})^M\langle u\rangle^M}{V^M + (\sigma/\hat{k})^M\langle u\rangle^M},\\ &= \omega_{\max} - (\omega_{\max} - \omega_{\min})\frac{\langle u\rangle^M}{U^M + \langle u\rangle^M},\end{aligned}$$

with $U^M = V^M(\hat{k}/\sigma)^M$ and we have rederived eq. (42). However, this calculation assumes linear kinetics for the $u \to v$ transition and $\sigma \ll k$. The reality is probably more complicated and further work must be done to see if these assumptions are justified. A starting point for calculating σ is by estimating the flux of NO into a smooth muscle cell (Vaughn et al., 1998).